Discovery of aza-aromatic anolytes for aqueous redox flow batteries via high-throughput screening

Qi Zhang[1,2], *Abhishek Khetan*[1,3], *Elif Sorkun*[1], *Süleyman Er*[1*]

[1] DIFFER – Dutch Institute for Fundamental Energy Research, De Zaale 20, 5612 AJ Eindhoven, The Netherlands
[2] SIAT – Shenzhen Institute of Advanced Technology, Chinese Academy of Sciences, Xueyuan Road 1068, 518055, Shenzhen, China
[3] MODES - Fuel Science Center, RWTH Aachen University, 52062 Aachen, Germany
[*] E-mail: s.er@differ.nl

Keywords: High-throughput virtual screening; Density functional theory; Redox flow battery; Material discovery

ABSTRACT

Aza-aromatics have recently emerged as a propitious class of electroactive compounds for energy storage in aqueous redox flow batteries (ARFBs). Here, using high-throughput virtual screening (HTVS), we explored a focused chemical subspace of aza-aromatics to determine the top performing candidates as anolytes in ARFBs. First, we designed a virtual chemical library that contains 13,406 aza-aromatic redox pairs, which was populated through the chemical functionalization of alloxazine, phenazine, and indigo backbones with five different R-groups that are known to affect the key battery properties. Then, we predicted the redox potential, aqueous solubility, and the likelihood of decomposition due to the undesirable hydration and tautomerization reactions of the compounds. An analysis of the decomposition thermodynamics of the aza-aromatic subclasses revealed differing correlations between the redox properties and the chemical stability of the compounds, where the latter is found to strongly depend on the type and quantity of the functional groups. Consequently, a total of 516 anolyte candidates that have lower redox potential and higher solubility than a typical anolyte compound, alloxazine 7-carboxylic acid (ACA), have been identified. Additionally, an automated vendor search for the HTVS-predicted top-performing compounds yielded two molecules that are readily purchasable for experimental validation. Finally, an analysis of the quantitative structure-property relationships showed that the mid-sized aza-aromatics, which are not well-explored in experiments, achieved the largest property tunability windows. Based on the new findings, we also propose a molecular engineering strategy in a way to balance the inherent trade-offs among the redox, solubility and chemical stability features of the aza-aromatic anolytes for ARFBs.

1. Introduction

The use of renewable solar and wind power has been significantly growing over the last decade, while the intermittency of the renewable energy sources remains to be a major challenge for their larger-scale application.[1–3] To address this challenge, aqueous redox flow batteries (ARFBs) that are based on novel chemistries are increasingly been researched as cost-effective and safe energy storage technology.[2,4] Aza-aromatics, which contain two redox active nitrogen atoms in aryl rings, have received recent interest for application in ARFBs.[5] The aza-aromatic family of compounds, including alloxazines[6,7] phenazines[8–10], indigos[11,12] can undergo various redox reactions that are shown in Fig. 1, and therefore, they can potentially function as the anolyte or catholyte in ARFBs.

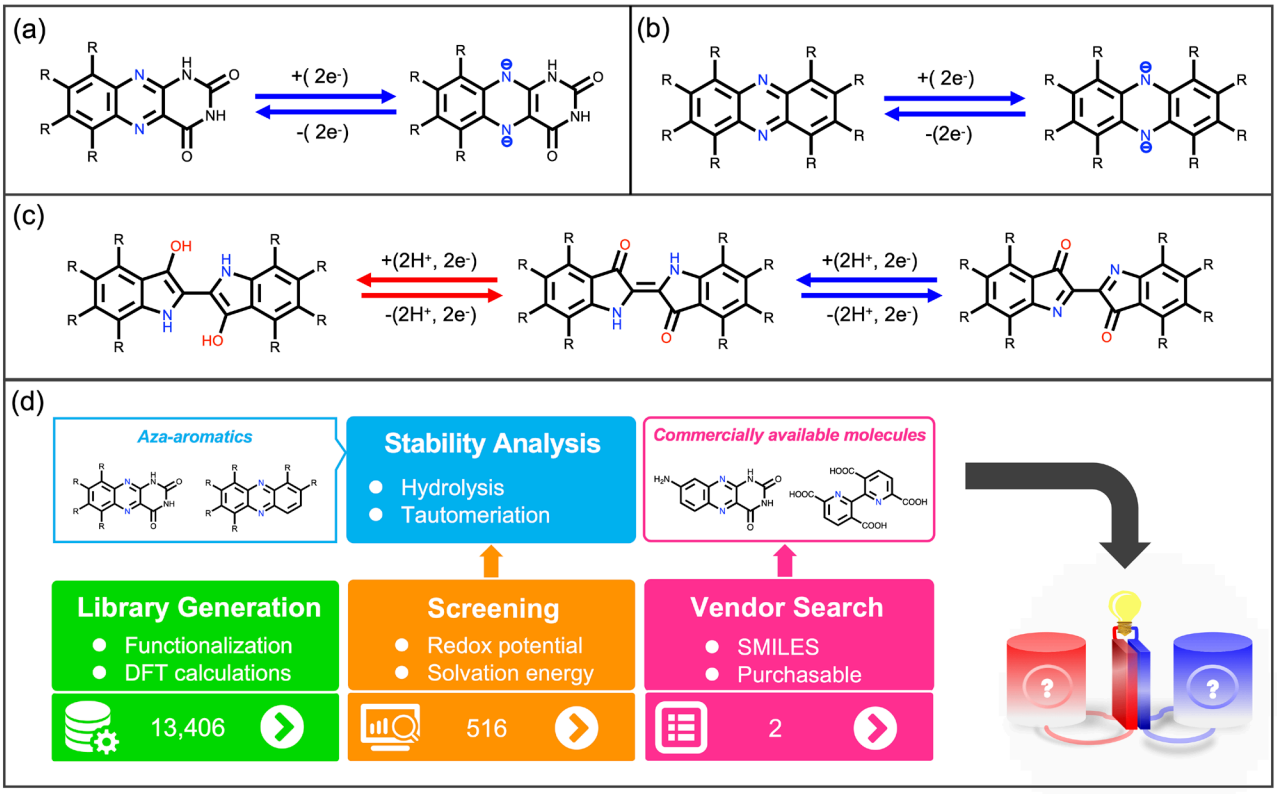

Fig. 1 The reversible redox reactions are shown for three representative aza-aromatic molecules in (**a**) alloxazine and its derivatives that undergo a two-electron process in alkaline medium,[6] (**b**) phenazine and its derivatives that undergo a two-electron process in alkaline medium,[8] (**c**) indigo and its derivatives that undergo two sets of two-electron two-proton redox reactions in acidic and neutral

conditions, respectively,[11] wherein only the reaction indicated by blue arrows is considered in the current study. An overview of the HTVS workflow, as well as the 2D structural representations of the HTVS-identified promising and purchasable anolyte molecules for ARFBs, are shown in **(d)**.

The battery-relevant properties of aza-aromatic molecules, including redox potential, solubility, and stability, need to be improved significantly for future commercialization.[6,8] High throughput virtual screening (HTVS) has increasingly been used as an effective tool for the discovery and design of aza-aromatic materials for ARFBs.[6,13–15] In this way, the battery-relevant properties can be systematically tuned by the functionalization of candidate electroactive compounds with a diverse set of electron-withdrawing/donating chemical groups.[6,8] To the best of our knowledge, a systematic HTVS study for the exploration of the chemical sub-space that contains small-to-medium and non-aryl aza-aromatics has not yet been performed. In parallel, owing to a limited number of experimental studies aimed at the use of aza-aromatics as electroactive materials in ARFBs, the structure-property relationships that would provide insight on the effects of various electron donating/withdrawing chemical groups, heteroatom substituents, and molecular sizes on the key ARFB performance metrics are not well established.

Here, to accelerate the discovery of promising aza-aromatic electroactive compounds for ARFBs, we performed a HTVS study on a comprehensive virtual library of diversified aza-aromatic chemistries. A schematic overview of the HTVS workflow is shown in Fig. 1d. The backbone structures used to build the library are inspired by the experimentally top-performing aza-aromatic motifs, including alloxazines, phenazines and indigos.[6,8–11,16] The generated library includes both 5- and 6-membered rings, their fused variations, as well as the heterocyclic molecules that are obtained by the substitution of ring carbon atoms with heteroatoms (Fig. 2). The redox potentials of the candidate molecules are predicted by employing a hierarchical computational workflow that includes density functional theory (DFT) calculations.[17,18] The aqueous solubility of the candidate molecules is

estimated by using the DFT-calculated solvation energy of the compounds as a proxy[14,19,20]. After a screening based on the calculated redox potential and solvation energy, we identified 516 promising candidates for experimental validation, while two molecules are directly purchasable upon performing an automated search on the vendor databases.[21] In addition to these results, we observed systematic correlations between the chemical stability and redox potential of the compounds, which indicate the presence of inherent trade-offs that would eventually need to be overcome in order to achieve a high battery performance. Thus, the HTVS performed in this study not only provides several candidate molecules that can potentially offer improved performance when compared to the best performing anolytes from literature, but also elucidates interesting molecular design principles that may be extrapolated to a much larger chemical space of aza-aromatic molecules than has been considered here.

2. Methods

2.1. Molecular library design

The molecules in the virtual library were created by functionalizing backbone structures starting from a set of six known molecules shown in Fig. 2a (molecules 1–6 with grey background). To systematically explore the chemical space of aza-aromatics, other molecules of 5- and 6-membered rings (7–31) were constructed as based on motifs emerging from the known structures. All backbones were systematically functionalized with chemical groups to generate a large screening library of molecules with expectantly wide-ranging electrochemical and thermochemical properties.

Molecule 1 is the oxidized form of indigo, which has been used as electrolyte material in ARFBs.[11,22] Molecules 2,[23] 3 and 4[24] are variations on molecule 1, in which carbonyl groups are replaced by O, C, and S atoms, respectively. Molecule 5 is alloxazine, which has previously been investigated as a solid-state anode material for non-aqueous lithium- and sodium-ion batteries,[25] while its functionalized derivatives have also shown good performance in ARFBs.[6,7] Molecule 6 is 2,2'-bipyridine, which is widely used as a ligand[26] for the synthesis of organic molecules and

pharmaceutical intermediates.[27,28] In addition, it has also been investigated as a candidate energy storage compound.[29]

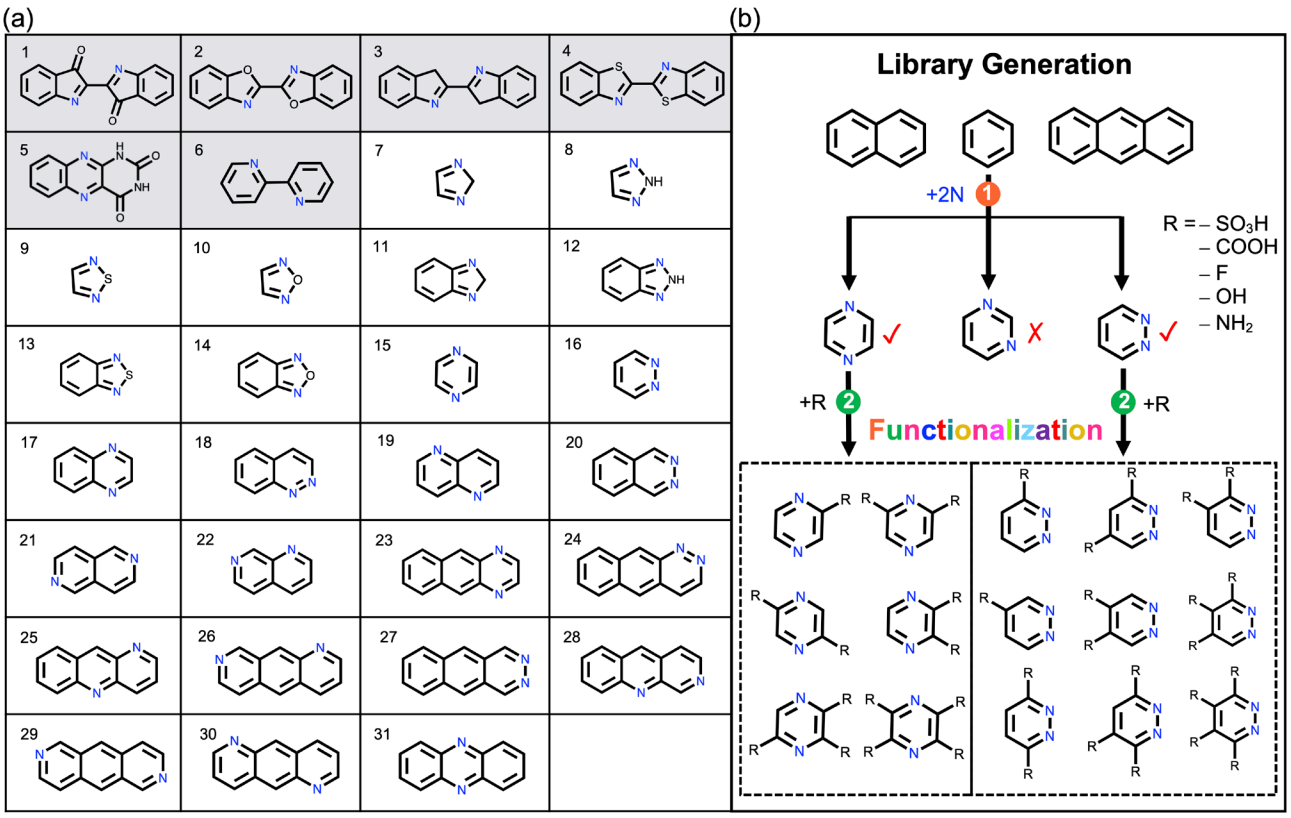

Fig. 2 (a) The 2D structural representations of reactant backbones that have been considered for HTVS in the current study. **(b)** A schematic representation of molecule functionalizations that have been applied during the enumeration processes of virtual molecular library generation.

For the backbone structures with 5-membered rings (7–14), the single C atoms that are positioned between the two N atoms of 2H-imidazole (7) and 2H-benzimidazole (11) molecules were substituted in turn with N, S, and O atoms, thereby generating two subsets (8–10 and 12–14) of heterocyclic backbones. The rest of the backbone structures (15–31) contain only 6-membered rings, and were created by using the Elemental Enumeration tool of the Schrödinger Materials Science Suite (SMSS).[30] In this process, two C atoms were substituted with two N atoms in three types of aromatic rings, namely, benzene, naphthalene, and anthracene. An example enumeration process is shown in

Fig. 2b for benzene. The enumeration process was performed exhaustively in order to fully cover the chemical subspace. Then, the duplicates were identified and removed. Next, the backbone structures that do not meet the requirement of a two-electron-backwards-aromatization reaction on the two N atoms were eliminated. These are cases in which the two N atoms are separated by an even number of conjugated bonds, which lead to the formation of radical C atoms upon reduction of the N atoms. We note that some of the generated backbones (15,[31] 17[32] and 31[8]), were experimentally tested in previous studies.

For the functionalization of the backbone structures, five chemical (R)-groups (–SO_3H, –COOH, –F, –OH and –NH_2) were used. These R-groups were chosen as based on their ability to tune the redox potential and aqueous solubility of the small electroactive compounds.[19,22] Next, an exhaustive enumeration of the functionalized derivatives of the reactant backbone structures was performed by using the Custom R-group Enumeration tool of SMSS.[30] A representation of the combinatorial generation of the functionalized molecules is shown in Fig. 2b. Lastly, the redox product molecules were generated according to a two-electron reaction mechanism (Fig. 1).[6,8,11] Accordingly, the virtual molecule library contains a total of 13,406 aza-aromatic redox pairs.

2.2. Computational methods

All DFT calculations were performed, by using the Jaguar package[33] as implemented in SMSS, on the lowest energy conformers of the molecules. To perform the geometry optimizations in the gas phase, the PBE exchange-correlation functional[34,35] and LACVP^{**++} basis set with polarization and diffuse functions[36] were used. The single point energies of the molecules were calculated in an implicit aqueous medium based on the Poisson-Boltzmann solvation model.[33,37] It has been shown that the lowest unoccupied molecular orbital (LUMO) energy of the reactant molecules was a good performing predictor of the measured redox potentials in experiments.[18] Accordingly, the equation used for predicting the redox potentials of aza-aromatic molecules is:

$$E^{o} = -0.376[E_{\mathrm{LUMO}}] - 1.726 \text{ (at pH = 7)} \quad (1)$$

where $[E_{\mathrm{LUMO}}]$ represents the DFT-calculated LUMO energy of the reactant molecule,[18] while the coefficients of Eqn. (1) are fitted to experimental data on 21 redox aza-aromatic redox couples that includes 17 alloxazine and 4 phenazine-like molecules.

With regards to aqueous solubility, it must be noted that solubility is a complex function of crystal packing free energy, which is described by the thermodynamic relation:

$$S = p^{o}\exp(-(\Delta G^{*}_{\mathrm{sub}} + \Delta G^{o}_{\mathrm{solv}})/RT)/RT \quad (2)$$

where $\Delta G^{*}_{\mathrm{sub}}$ is the sublimation free energy, $\Delta G^{o}_{\mathrm{solv}}$ is the solvation energy, p^{o} is standard pressure (1 atm), T is room temperature (298.15 K) and R is molar gas constant (8.314 J/(mol·K)). Usually, $\Delta G^{*}_{\mathrm{sub}}$ is extremely difficult to predict for organic molecules[38] due to the lack of knowledge about their crystal structures. In this work, the solvation energy, $\Delta G^{o}_{\mathrm{solv}}$, is used as a proxy for the prediction of solubility in aqueous media,[14,19,20] which is the difference between the solution phase energy and the gas phase energy of the compound. Thus, a large negative $\Delta G^{o}_{\mathrm{solv}}$ indicates a molecule with high aqueous solubility. In pursuit of water-soluble energy storage compounds, we calculated $\Delta G^{o}_{\mathrm{solv}}$ for the reactant molecules only, since they would expectedly be less soluble than their corresponding product molecules in aqueous solution.[19]

To further evaluate the effect of functional groups on the chemical stability and the redox behavior of compounds, we studied two representative backbone structures, 5[25] and 31[8], as inspired by their demonstrated good lab-performance in ARFBs. For alloxazine-based molecules, hydrolysis[6,39] has been proposed as the primary decomposition mechanism. In this reaction, the introduction of water to the amidic carbonyls results in a hydration step that is followed by a ring-opening step in the aqueous

solvent (Fig. 3a). Since the hydration step is the rate-limiting step[6], as a descriptor for the propensity of decomposition via hydrolysis of the alloxazine-based derivatives, we calculated the Gibbs free energy for hydration, $\Delta G^{\mathrm{h}}_{\mathrm{solv}}$, by using the following equation:

$$\Delta G^{\mathrm{h}}_{\mathrm{solv}} = G_{\mathrm{int}} - G_{\mathrm{reac}} - G_{\mathrm{H_2O}} \tag{3}$$

where G_{reac} is the Gibbs free energy of reactant (i.e., pristine) molecule, G_{int} is the Gibbs free energy of the hydrated intermediate, and $G_{\mathrm{H_2O}}$ is Gibbs free energy of H_2O molecule.

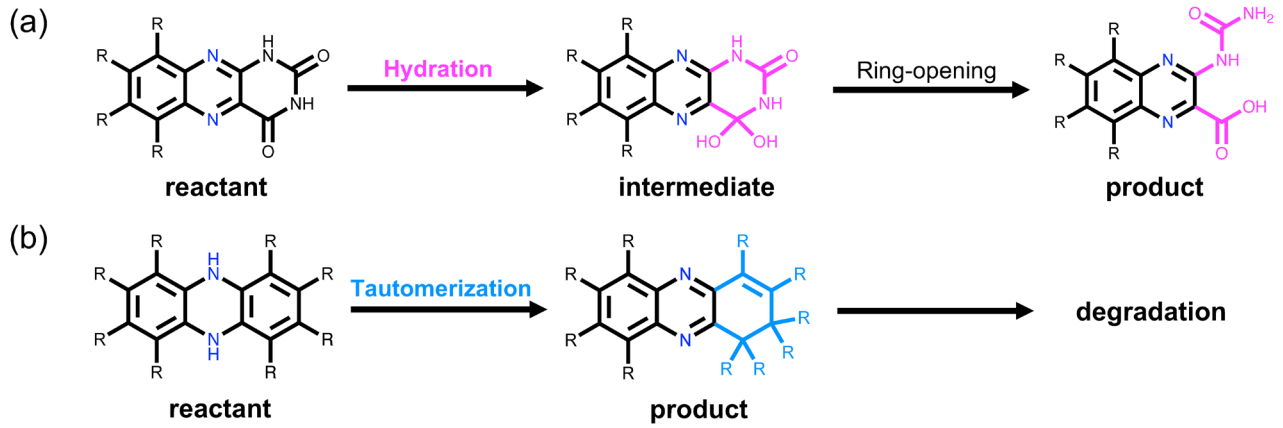

Fig. 3 The two possible reaction mechanisms that are related with the chemical instability of the compounds: **(a)** the hydration facilitated ring-opening of alloxazines, **(b)** the tautomerization of phenazines.

For phenazine-based molecules, the decomposition has been proposed to occur via tautomerization,[10] in which a formal migration of hydrogen atoms occurs together with a transition between a single and a double bond, as shown in Fig. 3b. During this reaction, the reduced electrochemical product of phenazine undergoes de-aromatization of the phenyl ring on the edge. The formation of the tautomer results in a direct loss of the active material, and thus, a capacity fade during electrochemical cycling experiments. The reverse process of re-aromatization back to the phenyl ring

is energetically unfavorable and often requires catalysts to overcome the reaction barrier.[40,41] To estimate the stability of phenazine-based molecules, we calculated the Gibbs free energy for tautomerization, $\Delta G^{\mathrm{t}}_{\mathrm{solv}}$, by using the following equation:

$$\Delta G^{\mathrm{t}}_{\mathrm{solv}} = G_{\mathrm{prod}} - G_{\mathrm{reac}} \quad (4)$$

where G_{reac} is Gibbs free energy of the reactant and G_{prod} is Gibbs free energy of the product molecules (Fig. 3b). Therefore, according to the two different mechanisms shown in Fig. 3, the more negative $\Delta G^{\mathrm{h}}_{\mathrm{solv}}$ and $\Delta G^{\mathrm{t}}_{\mathrm{solv}}$ are for a compound, the more likely that it will be chemically instable against the hydration and tautomerization reactions, respectively.

3. Results and discussion

3.1. Screening of available candidates with desired properties

Fig. 4 shows the distribution of the predicted redox potential, E^{o}, and solvation energy, $\Delta G^{\mathrm{o}}_{\mathrm{solv}}$, for all the molecules in the virtual library. Based on recent experiments, the molecules alloxazine-7-carboxylic acid (ACA)[6] and 7,8-dihydroxyphenazine-2-sulfonic acid (DHPS)[8] represent the best performing alloxazine and phenazine-based ARFB anolyte molecules, respectively. As criteria for screening, we used the DFT-calculated E^{o} (–0.188 V *vs.* RHE at pH = 7) and $\Delta G^{\mathrm{o}}_{\mathrm{solv}}$ (–23.08 kcal/mol) of ACA. Screening only on basis of redox potentials, a total of 8,834 redox couples (~66% of the virtual library) are found to have lower E^{o} than ACA. However, it must be noted that molecules with redox potential lower than –0.41 V would likely be unsuitable for application at pH = 7 due to the undesired H_2 evolution reaction.[21] Next, screening only on basis of solvation energy, a total of 6,091 molecules (~45 %) are predicted to have higher solubility (i.e., more negative $\Delta G^{\mathrm{o}}_{\mathrm{solv}}$ values) than that of ACA, which implies the presence of a wide chemical space for tuning solubility. Using the combined screening criteria (–0.41 V < E^{o} < –0.19 V *vs.* RHE at pH = 7 and $\Delta G^{\mathrm{o}}_{\mathrm{solv}}$ < –23.08

kcal/mol), a total of 516 aza-aromatic molecules are shortlisted as anolyte candidates. The full list of candidate molecules is shown in Supporting Information Table S1. These findings reveal a sizeable space of potentially high-performance molecules that is chiefly populated by molecules that are functionalized with –COOH group. In the distribution map shown in Fig. 4, it is observed that molecules with groups –F (green), –OH (blue) and $–NH_2$ (red) show three noticeably separate clouds: in –0.25 V < E^o < 0.2 V, –0.4 V < E^o < –0.25 V and E^o < –0.4 V. The molecules found in the topmost region are derivatives of backbone molecule #1 (oxidized form of indigo), which has an overall higher redox potential than other backbones. The molecules found in the middle region are derivatives of benchmark molecule #5 (ACA). While there are other distribution clouds, they are not directly apparent due to thousands of overlapping data points.

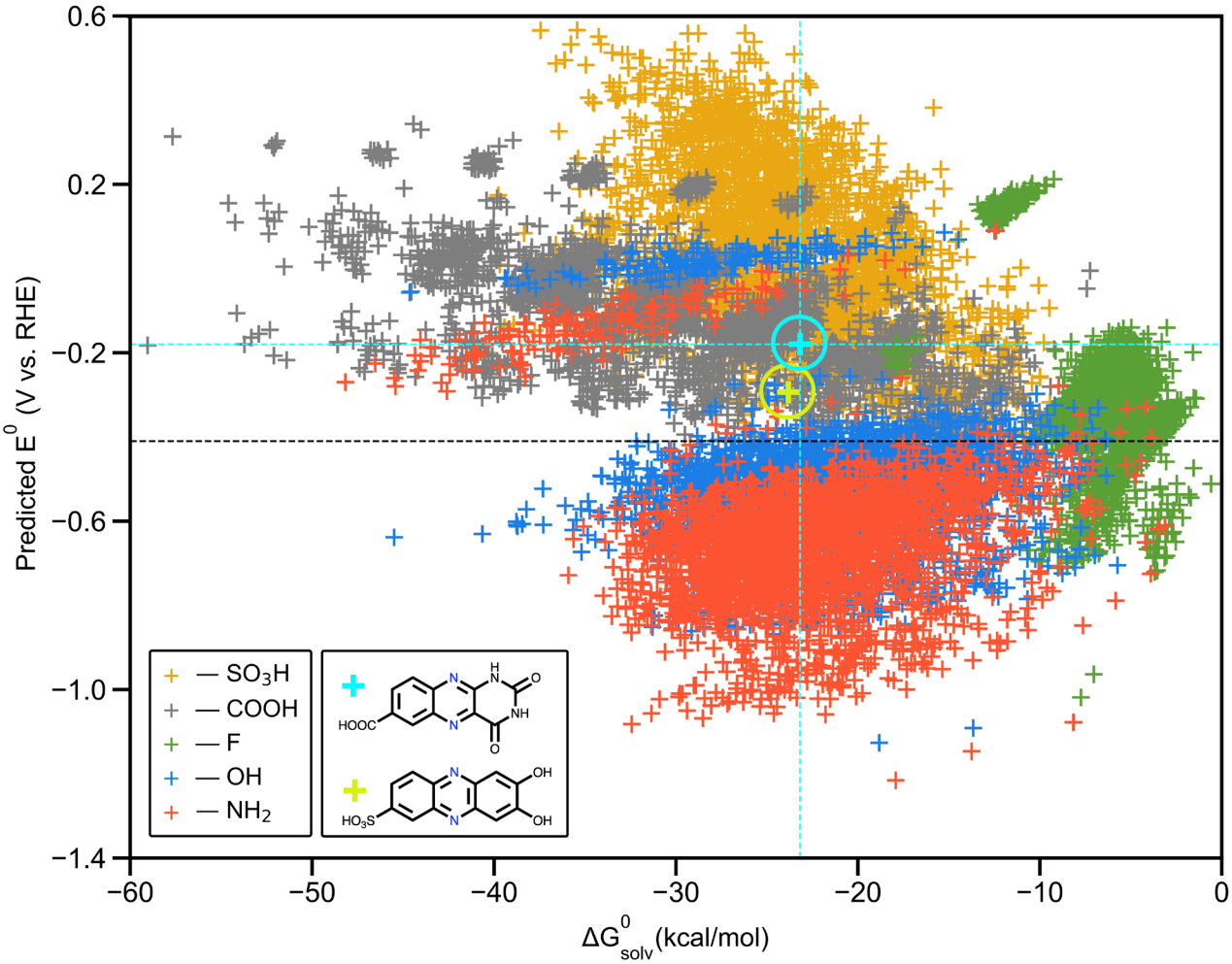

Fig. 4 The DFT-calculated E^{o} and ΔG^{o}_{solv} data of all molecules of the virtual chemical library. The molecules that are functionalized with the same chemical group are shown with a representative group color, which is shown in the bottom-left corner. The calculated values for the benchmark ACA molecule are shown with a cyan-colored cross. The accompanying cyan-colored dashed lines are used to guide the eye. The calculated values for the DHPS molecule are shown with an olive-colored cross. The horizontal dashed black line at E^{o} = –0.41 V represents the lowest acceptable redox potential value for ARFB anolytes at pH = 7.

To access the purchasability information of the shortlisted 516 aza-aromatic compounds, an exact SMILES-based search was performed in the ZINC database.[21] A client-side code[42] was developed to communicate with the ZINC servers, such that, when there existed a ZINC ID of the

searched SMILES representation, both the ZINC ID and corresponding page of the molecule were read by an *in-house* developed parser script. This way, commercial availability information, including stock status and list of vendors, were extracted and tabulated. As a result of the vendor search, the 2,2′-bipyridine-3,3′,6,6′-tetracarboxylic acid and 8-aminobenzo[*g*]pteridine-2,4(1H,3H)-dione molecules (Fig. 1d) were identified as the readily purchasable molecules for experimental testing.

Next, we singled out two backbone structures: (**a**) alloxazine (5)[6] and (**b**) phenazine (31)[10] in relation to their the outstanding electrochemical performance observed in experiments and we studied them in more detail. For alloxazine-based derivatives shown in Fig. 5a, with alloxazine indicated as molecule 5, it is observed that all groups, with the exception of –F, lead to more negative $\Delta G^{\circ}_{\mathrm{solv}}$. The $–SO_3H$ and –COOH groups increase E°, whereas –OH and $–NH_2$ groups have the opposite effect. Even after taking into account a hard low limit of –0.41 V, we find several new molecules decorated with –OH or $–NH_2$ groups that have the promise to perform better than their backbone structures both with respect to redox potential and solvation energy. In Fig. 5a, the experimentally validated alloxazine-based molecules are shown with A (alloxazine 7-carboxylic acid), B (8-hydroxyalloxazine), C (lumichrome), and D (7,8-dimethoxyalloxazine). As observed in Supporting Information Fig. S1a, for all the validated alloxazine-based molecules, the predicted redox potentials are quite consistent with the experimental measurements.[6] For phenazine-based derivatives shown in Fig. 5b, with phenazine indicated as molecule 31, the trends in redox potential and solvation energy are similar to the ones of alloxazine-based derivatives. After taking into account the low limit of –0.41 V, we find new molecules that are functionalized with the –OH group that have the potential to perform better than their backbone structures both with respect to redox potential and solvation energy. The validated phenazine-based molecules are shown in Fig. 5b with E (2,3-dihydroxyphenazine), F (2-amino-3-hydroxyphenazine), G (7,8-dihydroxyphenazine-2-sulfonic acid), H (7,8-dihydroxyphenazine-2-carboxylic acid), and I (benzo[a]hydroxyphenazine-7-carboxylic acid). As shown in Fig. S1b, the predicted E° of phenazine-based molecules do not agree well with their experimental values. The

disagreement can possibly due to the different conditions applied in the two different experimental studies.[8,9] This is unlike the case for alloxazine-based molecules in which the data of molecules was collected from the same source.[6] The voltammetry measurements for molecules 31, E, G, and H were performed with an anolyte concentration of 8.5 mM in 1.0 M NaOH solution[8], whereas for molecules F and I they were performed with an anolyte concentration of 2 mM in 1.0 M KOH solution.[9] To justify this argument further, we point to very recent study by Zhang et al. [43], which also predicted redox potentials of phenazine molecules published in recent years and their equation for potential prediction using $[E_{\mathrm{LUMO}}]$ is given as:

$$E^{\mathrm{o}} = -0.317[E_{\mathrm{LUMO}}] - 1.382 \text{ (at pH = 7)} \quad (5)$$

Firstly, the quantitative similarity between the new Eqn. (5) and Eqn. (1) from this work is abundantly clear in both the slope and intercept. This implies that Eqn. (1) is within the range of reasonable accuracy for phenazines, and also that the conclusions and findings of this work do not change significantly. The value of $[E_{\mathrm{LUMO}} = -4.090]$ for the benchmark molecule ACA results in a redox potential of $E^{\mathrm{o}} = -0.188$ V vs RHE at pH=7 with Eqn. (1) and $E^{\mathrm{o}} = -0.085$ V with the new Eqn. (5). The difference of 0.1 V is rather insignificant, especially for HTVS purposes, because it is well within the typical range of DFT errors. Using Eqn. (5) for only the phenazine molecules from the virtual library, it can be observed in Fig. S3 that there is no change in any trends, which is quite expected. Further, there is an upward vertical shift in the distribution of redox potentials when using Eqn. (5) due to which a few previously recommended phenazine molecules have now redox potential higher than $E^{\mathrm{o}} = -0.188$ V and are thus out of the screened list of candidates. Also, there are some new molecules that now pass the screening criteria for preventing H_2 evolution (i.e., –0.41 V at pH = 7). The total number of phenazine molecules screened using Eqn. (1) are 407 and using Eqn. (5) are 490. In the least, these observations imply that while the recommended list of candidates may turn out to be slightly worse than the benchmark molecule ACA, they will be further from the possibility of H_2

evolution issues, which is desirable. Based on these observations, we argue that screening based on Eqn. (1) doesn't significantly affect the conclusions of this work.

Eqn. (4) was fitted to 19 phenazine molecules spread over a range of ~0.9 V with an $R^2 = 0.69$, whereas the 21 data points used for fitting the coefficients of Eqn. (1) spanned a range of a little under ~0.3 V with an $R^2 = 0.96$. The 19 data points used by them were obtained from four different literature sources. Molecules P1, P6, P7, P11, P12 and P13 from Fig. 1 of their work are exactly the same as molecules 31, E, F, G, H, and I, respectively, from our work as shown in Fig. S1b. Yet again, it is clear that despite training on a similar number of data points and over a wider range of potentials, the fit of Eqn. (5) is worse than of Eqn. (1). Therefore, the argument that using data from multiple sources leads to unsystematic errors that are extremely difficult to capture via simple linear models stands validated. While using a simple descriptor such as $[E_{\mathrm{LUMO}}]$ cannot always be relied upon to provide redox potential predictions within errors of kT ~26 meV for every molecule, yet is it highly effective for a first order screening of large number of molecules, which is the primary aim of our study.

Interestingly, molecules G, H and I have a mixture of functional groups, and their redox and solvation properties emerge as approximately the average of the properties of molecules with only a single type of functional group. This implies that the combination of different chemical groups on the same backbone structure can potentially be an effective strategy for balancing the tradeoffs between the sought properties of an energy storage compound.

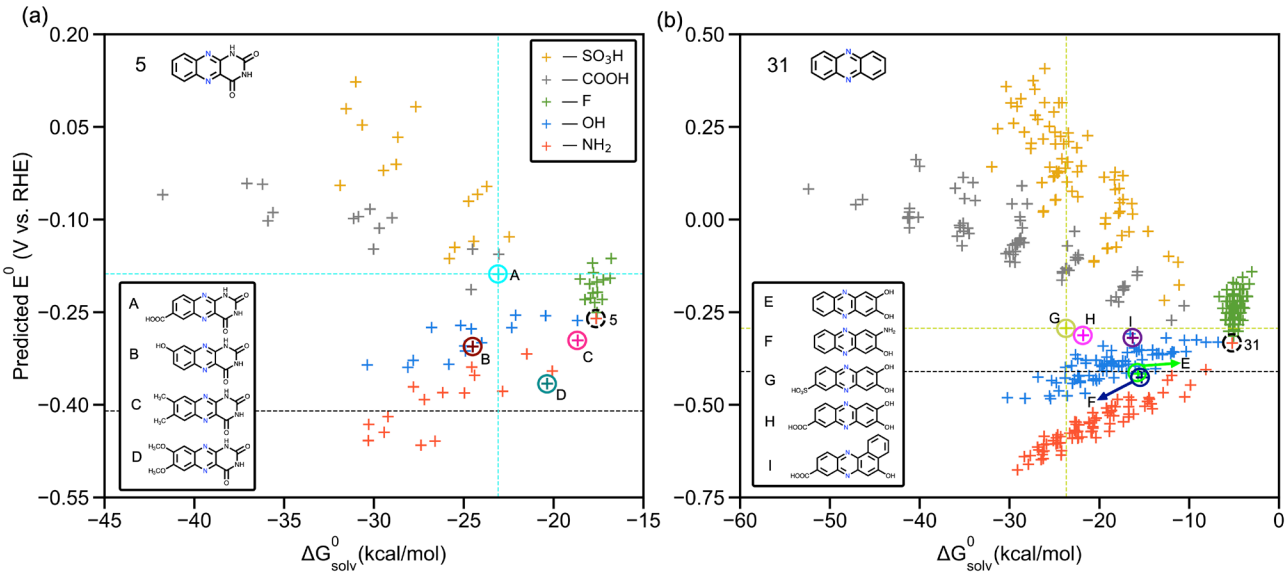

Fig. 5 The calculated E^{o} and ΔG^{o}_{solv} data for the backbone molecules of **(a)** alloxazine (5) and **(b)** phenazine (31). The calculated data for the molecules, which were previously experimented, are shown with colored crosshairs. The cyan- & olive-colored crosshairs and their accompanying dashed lines represent the calculated values for the benchmark molecules of A (ACA) and G (DHPS), in (a) and (b), respectively. The dashed black circles show the calculated values for the backbone molecules of (5) and (31), in (a) and (b), respectively. The molecules that were functionalized with the same chemical group are shown with a representative group color that is indicated in the top-right corner of (a). In both (a) and (b), the horizontal dashed black line at E^{o} = –0.41 V represents the lowest acceptable redox potential value for anolytes at pH = 7.

3.2. Structure-property relationships

3.2.1. Effect of functional group on the redox potential and solvation energy

We further studied the effect of various functional groups on E^{o} and ΔG^{o}_{solv}. For all backbone structures and their functionalized derivatives, the distributions of E^{o} *vs.* ΔG^{o}_{solv} are shown in Figs. 6, 7 and 8, respectively, for backbones from experimental literature, backbones that contain 5-membered rings, and backbones with only 6-membered rings.

As shown in Fig. 6, the electron-donating –OH and –NH_2 groups lower E^o, whereas the electron-withdrawing –F, –COOH and –SO_3H groups have the opposite effect. With regards to solvation energy, it is observed that all groups, except –F, lower the ΔG^o_{solv}. ΔG^o_{solv} is strongly influenced by the number and protonic character of the terminal H atoms on a molecule. The functional groups –OH, –NH_2, –COOH and –SO_3H have terminal H atoms that readily take part in H-bonding interactions, which will lead to more negative ΔG^o_{solv}. That is not the case for the –F substituted molecules. This argument is further supported at the end of this section, where we show that increasing the number of H containing functional groups leads to more negative ΔG^o_{solv}. While E^o of –OH and –NH_2 functionalized backbones are positively correlated with ΔG^o_{solv}, the correlation is opposite for –COOH and –SO_3H functionalized molecules. This allows, in principle, to use a combination of different functional groups such that the redox potential of these backbone structures can be altered relatively freely without being fully constrained by the undesirable effects on solubility.

Molecule 1, the oxidized form of indigo, has been used as an electrolyte in an ARFB in which the reduction occurs on the heterocyclic N atoms at 0.093 V *vs.* RHE (pH = 7).[11] The DFT-predicted value of 0.090 V *vs.* RHE (pH = 7) is consistent with this experimental redox potential. Upon functionalization, the redox potentials are found to spread over a wide range from ca. –0.3 V (with –NH_2) to ca. 0.6 V (with –SO_3H). Although the backbone structures 2 (–0.47 V), 3 (–0.43 V), and 4 (–0.46 V) have lower E^o than 1, they possess a highly similar spread upon functionalization. On the one hand, there are several molecules of these backbone structures that contain –NH_2 and –OH groups that are unsuitable candidates as active materials since their predicted redox potentials are lower than the H_2 evolution potential of –0.41 V. Yet, the same observation implies that the newly derived molecules from the backbone structures of 2, 3 and 4 provide a window for shifting towards more positive redox potentials, which could be a beneficial side effect for tuning other key battery material properties, including solubility and/or stability. Therefore, they are still quite worthy of synthesis and further experimental validation. The results for the backbone structure 5 (alloxazine) was discussed earlier in

Section 3.1. Lastly, the backbone structure 6 (–0.73 V) is predicted to have a very low E^o. Moreover, it surprisingly shows a largely tunable redox potential window, that is from –1.1 to 0.2 V, although it can accommodate only a small number of mutable positions. Similar to the arguments that have been made above for the other molecules of this group, the molecule 6 is worthy of synthesis and further experimental validation.

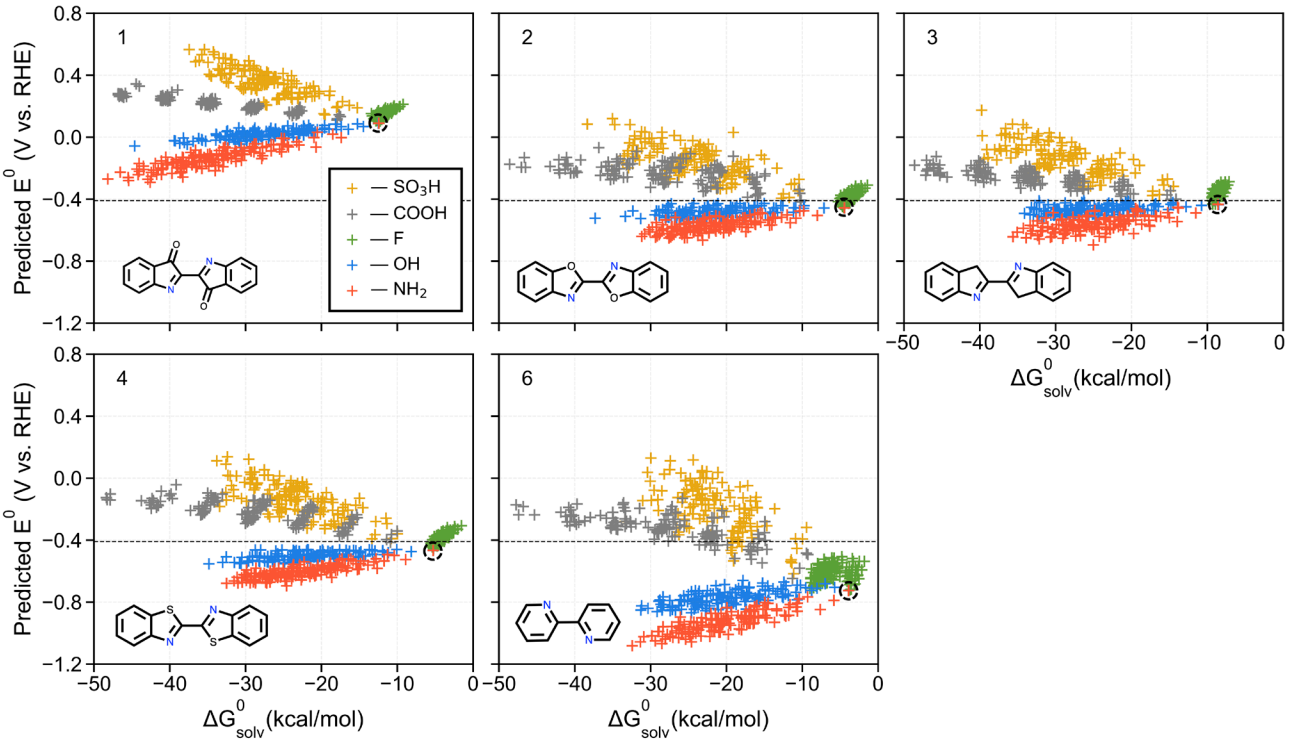

Fig. 6 The calculated E^o and ΔG^o_{solv} data for aza-aromatics of different sizes. The dashed black circles show the calculated values for the backbone molecules. The molecules that are functionalized with the same chemical group are shown with a representative group color that is given in the inset of molecule (1). The horizontal dashed black lines at E^o = –0.41 V represent the lowest acceptable redox potential value for anolytes in neutral media.

Next, as shown in Fig. 7, for the group of backbone structures with two reactive N atoms in 5-membered rings, the overall effect of functional groups on E^o and ΔG^o_{solv} is similar to that have been observed for backbone structures 1–6. When considering the effect of heteroatom substitution in

backbone #7, the substitution with N (#8) lead to drastically lower E^{o} and ΔG^{o}_{solv}, whereas the substitutions with S (#9) and O (#10) lead to slightly lower E^{o} but higher ΔG^{o}_{solv}. The shifts in redox potential due to heteroatom substitutions are cause by shifts in $[E_{LUMO}]$, which are in turn caused by electronic structure reorganizations. The reorganization results from the differences in electronegativity (χ), lone pairs and terminal H atoms of the heteroatoms, as well as the geometrical strain induced due to their presence. Starting with molecule #7, we note that the C (χ = 2.56) atom with two terminal H atoms is less electronegative than the neighboring N (χ = 3.04) atoms but it does not have any lone pairs. In comparison in molecule #8, the heteroatom N has the same electronegativity as the neighboring N atoms and has a lone pair and an electron donating terminal H atom. Consequently, the heteroatom N has an overall electron donating character that increases the $[E_{LUMO}]$ of the neighboring N atoms that take part in the redox reaction, and thus leads to much lowered redox potential of #8. In comparison in #10, the heteroatom O (χ = 3.44) is more electronegative than the neighboring N atoms, but the presence of two donatable lone pairs cancels the electron withdrawing effect. Thus molecule #10 has a slightly higher $[E_{LUMO}]$ and slightly lower redox potential compared to that of the unsubstituted molecule #7. Lastly in #9, the heteroatom S (χ = 2.58) with no terminal H atoms is less electronegative than the neighboring N atoms, and has very similar electronegativity to that of C. Although, the heteroatom S has two lone pairs in ring, it can also accept electrons to due to its ability to fill its empty 3d orbitals (which is why S can form up to 6 bonds). The overall result is a heteroatom S that is slightly more electron donating than C, thus leading to slightly higher $[E_{LUMO}]$ and slightly lower redox potential compared to that of the unsubstituted molecule #7.

To understand the effect on solvation energy (ΔG^{o}_{solv}) of molecule #7 due to heteroatom substitution with N (#8), S (#9) and O (#10), we argue that within the limits of the parametrized implicit solvation model, ΔG^{o}_{solv} can be understood as a function of the number and protonic (i.e., electron deficient) character of terminal H bonds, which are widely known to directly influence the solubility of any organic molecule. While the change in the delocalized electron density in the rings due to

heteroatom substitutions will also affect the ΔG^{o}_{solv} of the molecule, we argue that the number and protonic character of terminal H bonds are the dominating factors. To demonstrate this quantitatively, we calculated the maximum atomic electrostatic potential (ESP) of the terminal H atoms for the eight molecules under consideration, all by using the exact same simulation parameters for single point energy calculation as described in the Methods section. The ESP describes the protonic character of the terminal H atoms, including their local environment and interactions with the ring atoms. Consequently, the higher the ESP, the more is the protonic character of the terminal H atoms and thus the more negative is the energy of electrostatic interaction between the terminal H atoms and the partial negative charge on the oxygen atoms of the surrounding water molecules, which are represented here by the dielectric continuum. Further, to account for the varying number of terminal H bonds across the molecules, their total contribution is aptly taken as a cumulative sum of the individual atomic contributions. The calculated ESP values are shown in the Table S2. It can be clearly observed that the higher is the cumulative ESP for a given molecule, the more negative is ΔG^{o}_{solv}. These effects are partly dissimilar to the observations made in a previous work on quinone-like molecules,[22] in which both N and O substitution leaded to lower redox potential and higher solubility, whereas S substitution had an opposite effect. A more detailed comparison of heteroatom substitutions in aza-aromatic and quinone-like molecules is provided in Table S3.

Similar to the case of purely 5-membered rings, for the fused ring backbone structure 11, the heterocyclic substituted variations with N (12) lead to lower E^{o} and ΔG^{o}_{solv}. Similarly, the substitutions of S (13) and O (14) lead to lower E^{o} but higher ΔG^{o}_{solv}. Yet again, as shown in shown in Table S3, these effects are different from the previous observations for quinone-like backbones,[22] in which both N and O substitutions leaded to lower redox potential and higher solubility, whereas S substitution showed an adverse effect. Altogether, these results show that the heterogeneity brought on by the substitution of ring C atoms with N atoms is a potentially fruitful strategy for favorable tuning of the redox potential and solubility in small aza-aromatic type molecules.

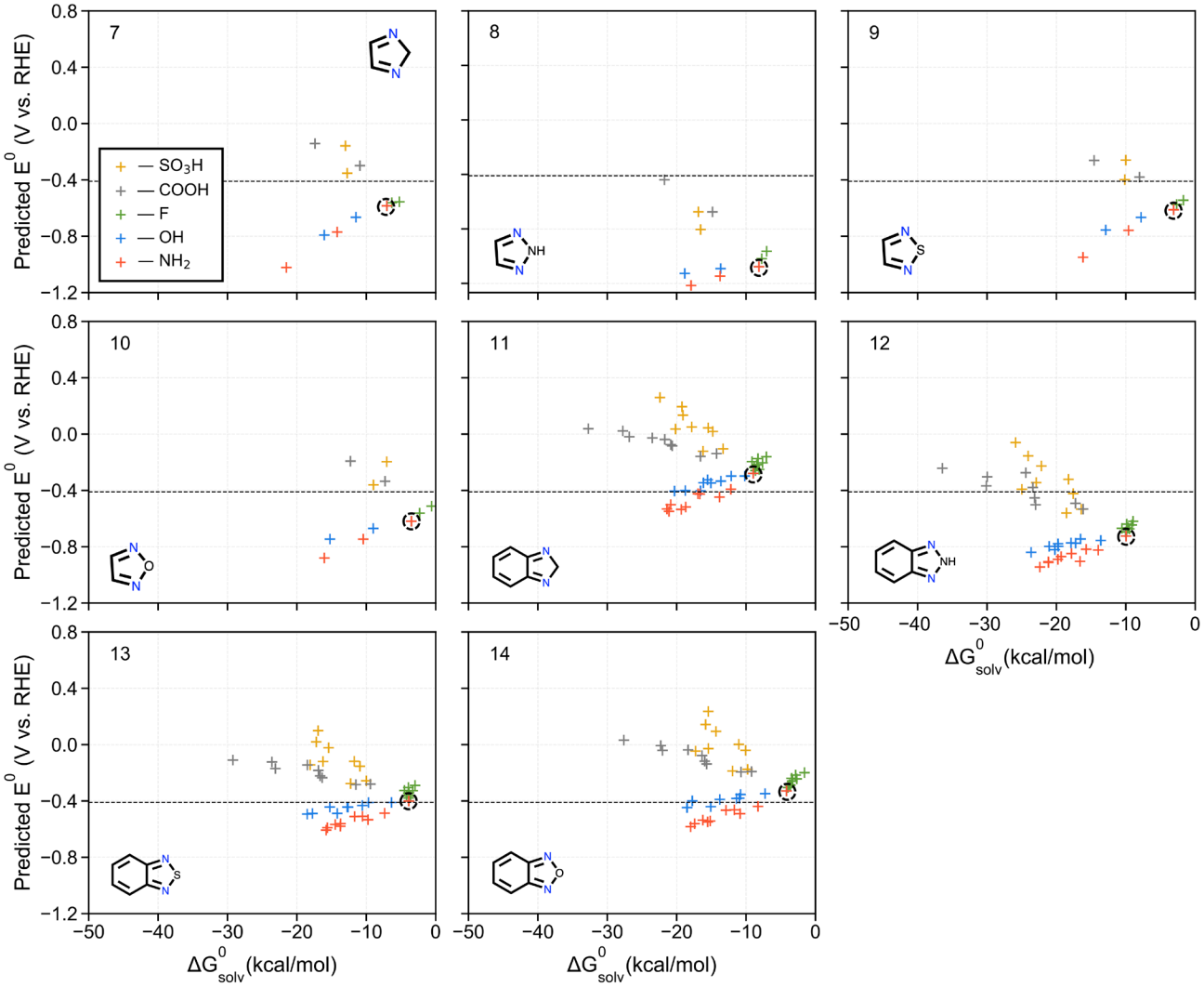

Fig. 7 The calculated E^{o} and ΔG^{o}_{solv} data for aza-aromatics that contain 5-membered rings. The dashed black circles show the calculated values for the backbone molecules. The molecules that are functionalized with the same chemical group are shown with a representative group color that is given in the inset of molecule (7). The horizontal dashed black lines at E^{o} = –0.41 V represent the lowest acceptable redox potential value for anolytes at pH = 7.

Next, for molecules from 15 to 31, which are comprised of 6-membered rings (molecules 15 and 16 are shown in Fig. S2, 17 to 30 in Fig. 8, and 31 in Fig. 5, respectively), a similar overall trend is observed as earlier with respect to the effect of functional groups on E^{o} and ΔG^{o}_{solv}. We found that

the redox potentials of single ring backbone structures, 15 and 16, are quite similar to each other. However, they are spread over a wider range for molecules with two (17–22) and three rings (23–31). The solvation energies for the backbone structures are also found to be a complex function of the size of the molecules and the distance between the backbone nitrogen atoms. A rather unsurprising result is that owing to a larger number of positions available for functionalization, the large-sized molecules show a wider range of tunability in redox potentials and solvation energies. It is also observed that when the two reacting N atoms are on the same outer edge (i.e., 3–4 positions) of a 6-membered ring (e.g., 16 in Fig. S2, 20 and 27 in Fig. 8) then the backbone structure has significantly low $\Delta G^{\mathrm{o}}_{\mathrm{solv}}$. The calculated E^{o} and $\Delta G^{\mathrm{o}}_{\mathrm{solv}}$ values for these compounds are shown in Table S4.

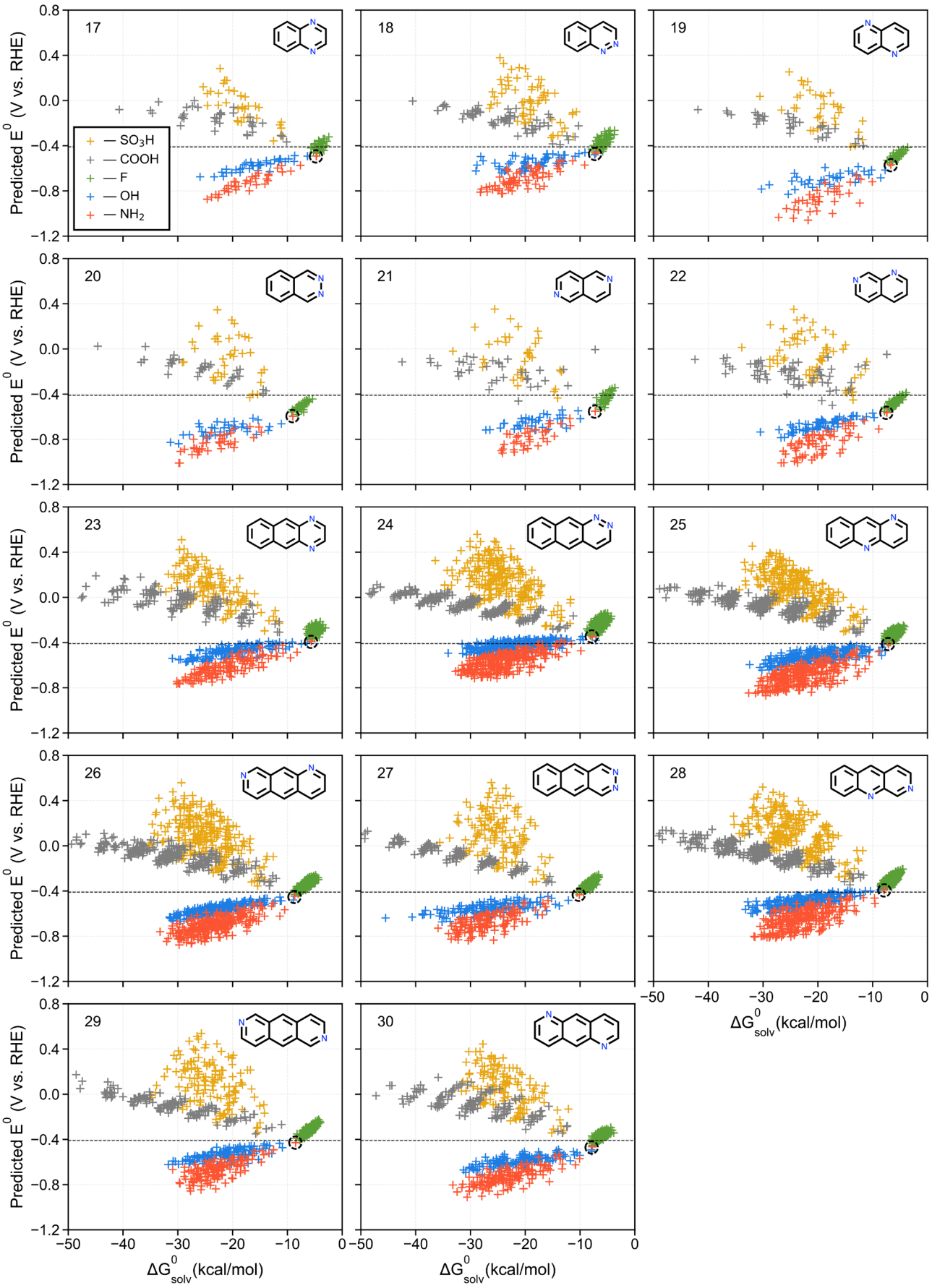
17
18
19
20
21
22
23
24
25
26
27
28
29
30
— SO3H
— COOH
— F
— OH
— NH2
Predicted E0 (V vs. RHE)
ΔG0solv (kcal/mol)
0.8
0.4
0.0
−0.4
−0.8
−1.2
−50
−40
−30
−20
−10
0

Fig. 8 The calculated E^{o} and ΔG^{o}_{solv} data for aza-aromatics that contain two or three fused 6-membered rings. The dashed black circles show the calculated values for the backbone molecules. The molecules that are functionalized with the same chemical group are shown with a representative group color that is given in the inset of molecule (17). The horizontal dashed black lines at E^{o} = –0.41 V represent the lowest acceptable redox potential value for anolytes at pH = 7.

Further, we analyzed the effect of the number of functional groups and ring size on E^{o} and ΔG^{o}_{solv}. Fig. 9 shows the results for one-ring (15–16), two-ring (17–22) and three-ring (23–31) molecules. It is observed that, regardless of the ring size, E^{o} (Fig. 9 (a, c, e)) and ΔG^{o}_{solv} (Fig. 9 (b, d, f)) vary monotonically with the number of functional groups. This finding implies that the properties of the backbone structures could be tuned in either direction simply by the addition or removal of an increasing number of functional groups of the desired kind. When considering only the backbone structures, the distributions of E^{o} (Figs. 9 (a, c and e)) show a strong dependence on the ring size. With increasing number of rings, the distribution of E^{o} shifts towards more positive values. This can be explained by the higher level of electronic conjugation that is present in aromatic molecules of increasing size. Differently, the spread of ΔG^{o}_{solv} (Figs. 9 (b, d and f)) with respect to number of rings does not show a clearly visible trend.

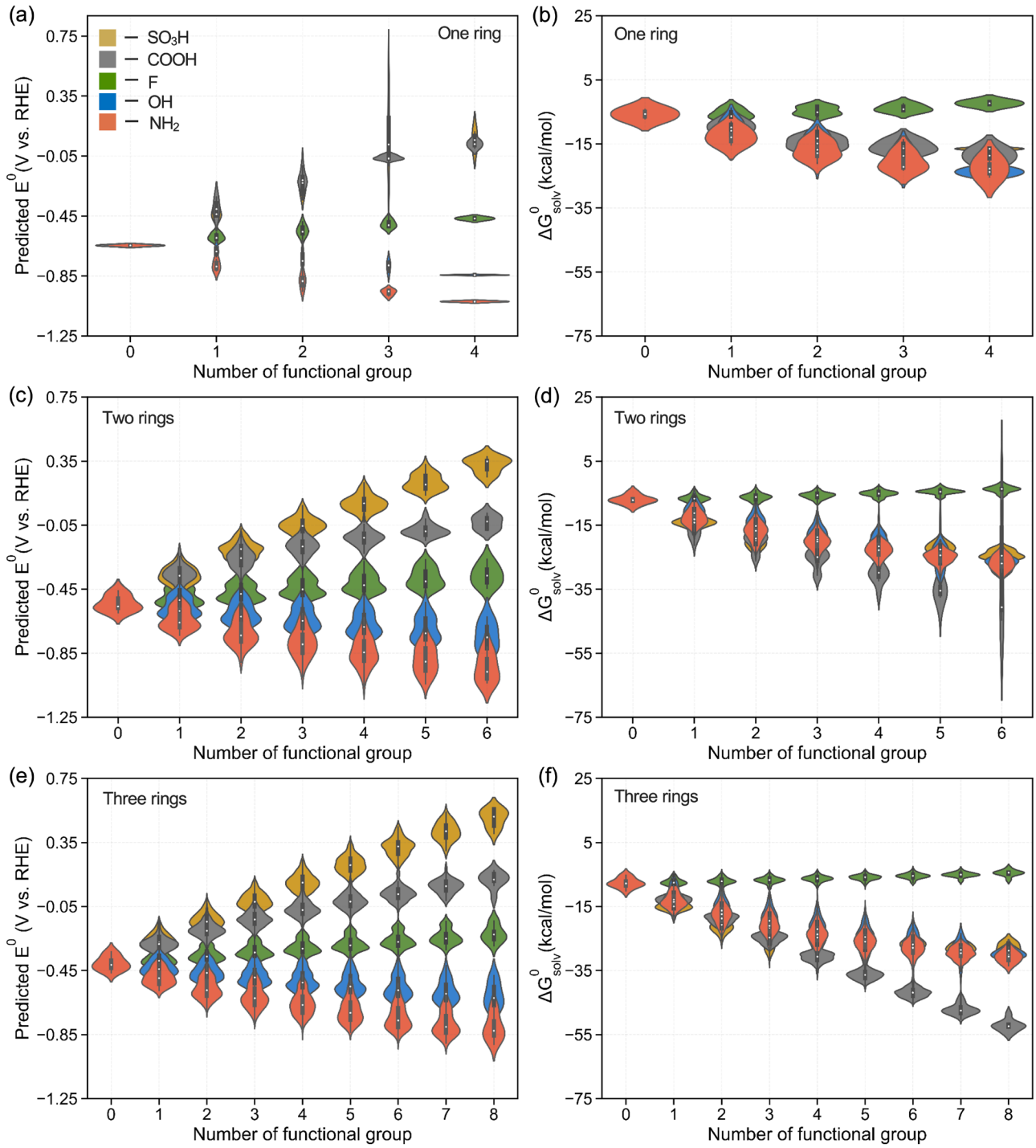

Fig. 9 The effects of the incremental R-group substitutions and ring numbers on E^{o} and ΔG^{o}_{solv} of the molecules. **(a)** and **(b)** show the effect of the number of R-group substitutions on E^{o} and ΔG^{o}_{solv} of the molecules that contain one ring (15 and 16); **(c)** and **(d)** show the effect of the number of R-group substitutions on E^{o} and ΔG^{o}_{solv} of the molecules that contain two rings (17–22); **(e)** and **(f)** show the effect of the number of R-group substitutions on E^{o} and ΔG^{o}_{solv} of the molecules that contain three

rings (23–31). The functional groups and ring sizes are highlighted in different colors. From (a) to (f), the molecules that are functionalized with the same chemical group are shown with a representative group color that is given in the inset of (a).

3.2.2. Stability of alloxazine and phenazine derivatives

The chemical stability of electroactive molecules is of critical importance to enable sustainable rechargeability and long lifespan. In this work, functionalization of aza-aromatic backbones with chemical groups has primarily been performed with an aim to tune their redox potential and solubility. Expectedly, there exist inherent trade-offs between redox potential, solubility, and chemical stability, which are not immediately apparent. Therefore, it is important to gain at least a preliminary understanding of the effect of functionalization on chemical stability of aza-aromatics. Given the recency of application of aza-aromatics in ARFBs with diverse electrodes and supporting electrolytes, it is particularly challenging to ascertain the mechanisms of their chemical decomposition. In order to have an understanding of chemical stability, we again singled out two backbone structures: (**a**) alloxazine[6] (5) and (**b**) phenazine[10] (31).

As described earlier, we calculated the Gibbs free energy for hydration ($\Delta G^{\mathrm{h}}_{\mathrm{solv}}$) and used it as a descriptor for estimating the propensity of decomposition of alloxazine derivatives via hydrolysis.[6,39] As shown in Fig. 10a, the calculated positive values of $\Delta G^{\mathrm{h}}_{\mathrm{solv}}$ show that this process is endothermic and it has loose but clear dependence on both the type and number of functional groups. Additionally, it is observed that high stability (i.e., largely positive $\Delta G^{\mathrm{h}}_{\mathrm{solv}}$) is loosely correlated with low E^{o}. As seen on the bottom-right of Fig. 10a, the electron-donating groups such as –OH and –NH_2, seem to be optimum choices for the functionalization of alloxazine molecules because they are very useful for decreasing the E^{o} and $\Delta G^{\mathrm{o}}_{\mathrm{solv}}$, as well as making the hydrolysis process thermodynamically less favorable.

It is worth noting that –NH_2 functionalized alloxazines have not yet been explored in experiments for energy storage and one such specimen is found to be commercially available in our vendor search. Figs. 10c and 10d show the dependence of the ΔG^{h}_{solv} and ΔG^{t}_{solv}, respectively, on the number of functional groups. In these figures, we also plot a dotted line joining the lowest energy isomers for a given number of functional groups to be able to draw some general conclusions. When looking at the lowest energy isomers, ΔG^{h}_{solv} of alloxazines shows a non-monotonic dependence on the number of functional groups (Fig. 10c) in which it first decreases and then increases with the number of functional groups. This type of dependence is found for all types of functional groups. For ΔG^{t}_{solv}, the dependence is clearly monotonic (Fig. 10d). However, ΔG^{t}_{solv} increases for –SO_3H and –COOH, whereas it decreases for –OH and –NH_2, while being nearly constant for –F.

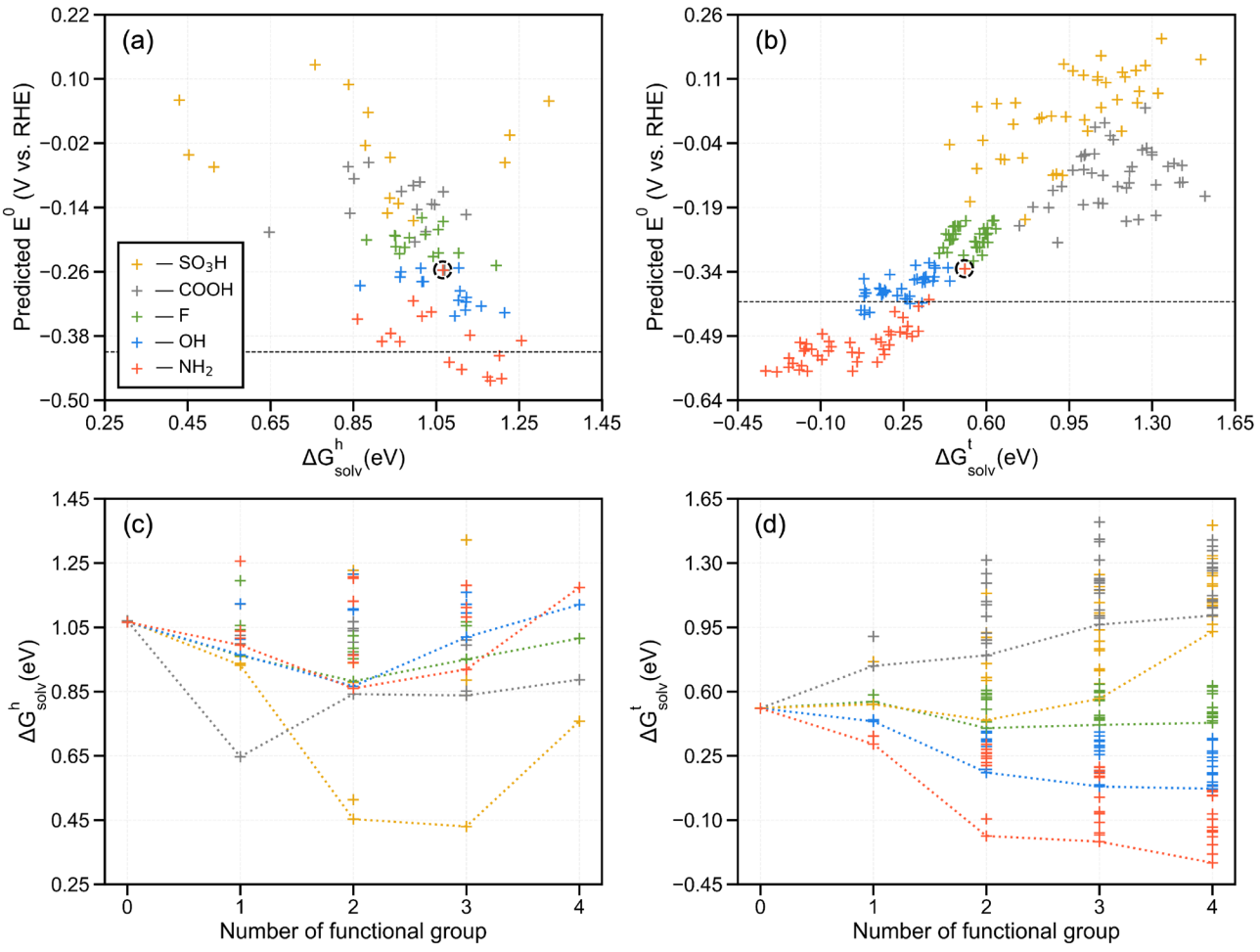

Fig. 10 The correlations between **(a)** E^{o} and ΔG^{h}_{solv}, when studying the decomposition of alloxazine-based molecules via hydration reactions, and **(b)** E^{o} and ΔG^{t}_{solv}, when studying the decomposition of phenazine-based molecules via tautomerization reactions, respectively. The plots **(c)** and **(d)** show the dependence of ΔG^{h}_{solv} and ΔG^{t}_{solv}, respectively, on the number of functional groups, in which the dotted lines connect the lowest energy isomers at a given number of functional groups. The molecules that are functionalized with the same chemical group are shown with the same representative group color that is given in the inset of (a). The horizontal dashed black lines at E^{o} = –0.41 V represent the lowest acceptable redox potential value for anolytes at pH = 7.

For estimating the propensity of decomposition of phenazine derivatives via tautomerization, we calculated and used the Gibbs free energy of tautomerization energy (ΔG^{t}_{solv}) as a descriptor. As shown in Fig. 10b, molecules with –OH have highly negative ΔG^{t}_{solv}, which indicates that they will likely be unstable against tautomerization. Followed by them are the molecules that contain $–NH_2$ groups. ΔG^{t}_{solv} also shows a clearly visible dependence on the type and number of functional groups. Unlike the ΔG^{h}_{solv} descriptor used for alloxazine molecules, high stability (i.e., largely positive ΔG^{t}_{solv}) is strongly correlated with high E^{o} for phenazines. As discussed earlier, the –COOH and $–SO_3H$ groups significantly increase the E^{o} of the functionalized molecules when compared to their respective backbone structures. For phenazine molecules, a rational strategy therefore would be to functionalize them with a mixture of groups such that the stability is not compromised while aiming for the low E^{o} values in ARFB anolytes.

4. Conclusions

In this work, we performed a HTVS study on a focused chemical space of small aza-aromatics, which included compounds of 5- and 6-membered rings and their fused variations with heterocyclic substitutions. The redox potentials of the candidates were predicted by applying a linear regression

model that employs the DFT-calculated LUMO energy of the reactant molecules as the descriptor, while the aqueous solubility of the compounds were approximated via the DFT-calculated solvation energy of the reactant molecules. We identified a total of 516 aza-aromatic molecules that are worthy of experimental validation in ARFBs, as they have lower redox potential and higher solubility when compared to the benchmark molecule ACA. Furthermore, an automated vendor search for the promising candidates yielded two molecules that are readily purchasable.

Next, a detailed analysis of the structure-property relationships by considering the effects of ring size, chemical functional groups and heteroatoms on the two important performance metrics of redox potential and aqueous solvation energy resulted in the following observations: (a) the electron-donating –OH and $–NH_2$ groups lower the redox potential, whereas the electron-withdrawing –F, –COOH and $–SO_3H$ groups have the opposite effect; (b) with the exception of –F, all groups (–COOH, $–SO_3H$, –OH and $–NH_2$) lower the solvation energy; (c) regardless of the ring size, increasing the number of functional groups on the molecules has a monotonous effect on both redox potential and solubility; (d) molecules substituted with new N heteroatoms have lower redox potential and more negative solvation energy, whereas the substitution of ring C atoms with S or O heteroatoms lead to lower redox potential and more positive solvation energy; (e) augmenting the number of rings on molecules, without introducing any additional functional groups, increases redox potentials but has no noticeable effect on solvation energies.

Finally, an analysis of the decomposition of alloxazine-based molecules via hydrolysis revealed that their chemical stability is determined by the type and number of functional groups. The introduction of electron-withdrawing groups (–OH and $–NH_2$) not only lowered the redox potential and solvation energy, but it also improved the stability of the backbone structures. Similarly, the decomposition of phenazine-based molecules via tautomerization was also found to be influenced by the type and number of functional groups. However, for the phenazine family of compounds, the chemical stability was positively correlated with the redox potential. Based on all of these findings,

we propose that combining chemical groups for functionalization can be a rational strategy to balance the trade-offs between redox potential, solvation energy, and chemical stability. The new findings from the current study are expected to support the meticulous molecule engineering efforts for efficient energy storage in ARFBs.

Supporting Information

The Supporting Information includes: (Fig. S1) The comparison of measured and predicted E^{o} values of ARFB molecules; (Fig. S2) The distribution of calculated E^{o} and $\Delta G^{\mathrm{o}}_{\mathrm{solv}}$ values for the 6-membered single-ring aza-aromatics; (Table S1) The SMILES representation, E^{o} and $\Delta G^{\mathrm{o}}_{\mathrm{solv}}$ values of the top 516 promising anolyte compounds for ARFBs; (Table S2) The calculated ESP data of H atoms on molecules; (Table S3) The comparison of heteroatom effects on E^{o} and $\Delta G^{\mathrm{o}}_{\mathrm{solv}}$ of the aza-aromatic and quinone-like backbones; (Table S4) The influence of growing number of rings in molecule backbones on the calculated E^{o} and $\Delta G^{\mathrm{o}}_{\mathrm{solv}}$ values.

Acknowledgements

We thank Prof. René Janssen for discussions. This research received funding from the Dutch Research Council (NWO), through the COLORFLOW project partnership of DIFFER and Green Energy Storage, in the framework of the Materials for Sustainability programme and from the Ministry of Economic Affairs in the framework of the "PPS-Toeslagregeling" grant no 739.017.013. A.K. acknowledges financial support in part by the Deutsche Forschungsgemeinschaft (DFG, German Research Foundation) under Germany's Excellence Strategy – Exzellenzcluster 2186 "The Fuel Science Center" ID: 390919832. S.E. acknowledges funding from the initiative "Computational Sciences for Energy Research" of Shell and NWO grant no 15CSTT05. This work was sponsored by NWO Exact and Natural Sciences for the use of supercomputer facilities.

ORCID

Qi Zhang: 0000-0003-1644-4944

Abhishek Khetan: 0000-0003-2260-8271

Elif Sorkun: 0000-0003-1693-6463

Süleyman Er: 0000-0002-5005-3894

References

1 H. Chen, G. Cong and Y. C. Lu, *J. Energy Chem.*, 2018, **27**, 1304–1325.

2 Y. Ding, C. Zhang, L. Zhang, Y. Zhou and G. Yu, *Chem. Soc. Rev.*, 2018, **47**, 69–103.

3 Z. Zhao, C. Zhang and X. Li, *J. Energy Chem.*, 2022, **67**, 621–639.

4 C. Zhang, L. Zhang, Y. Ding, S. Peng, X. Guo, Y. Zhao, G. He and G. Yu, *Energy Storage Mater.*, 2018, **15**, 324–350.

5 K. J. S. Elena I. Romadina, Denis S. Komarov and P. A.Troshin, *Chem. Commun.*, 2021, **57**, 2986–2989.

6 K. Lin, R. Gómez-Bombarelli, E. S. Beh, L. Tong, Q. Chen, A. Valle, A. Aspuru-Guzik, M. J. Aziz and R. G. Gordon, *Nat. Energy*, 2016, **1**, 16102.

7 J. J. Hasford and C. J. Rizzo, *J. Am. Chem. Soc.*, 1998, **120**, 2251–2255.

8 A. Hollas, X. Wei, V. Murugesan, Z. Nie, B. Li, D. Reed, J. Liu, V. Sprenkle and W. Wang, *Nat. Energy*, 2018, **3**, 508–514.

9 C. Wang, X. Li, B. Yu, Y. Wang, Z. Yang, H. Wang, H. Lin, J. Ma, G. Li and Z. Jin, *ACS Energy Lett.*, 2020, **5**, 411–417.

10 S. Pang, X. Wang, P. Wang and Y. Ji, *Angew. Chemie*, 2021, **133**, 5349–5358.

11 J. Carretero-González, E. Castillo-Martínez and M. Armand, *Energy Environ. Sci.*, 2016, **9**, 3521–3530.

12 A. Mukhopadhyay, H. Zhao, B. Li, J. Hamel, Y. Yang, D. Cao, A. Natan and H. Zhu, *ACS Appl. Energy Mater.*, 2019, **2**, 7425–7437.

13 R. P. Fornari, M. Mesta, J. Hjelm, T. Vegge and P. De Silva, *ACS Mater. Lett.*, 2020, **2**, 239–246.

14 L. Cheng, R. S. Assary, X. Qu, A. Jain, S. P. Ong, N. N. Rajput, K. Persson and L. A. Curtiss, *J. Phys. Chem. Lett.*, 2015, **6**, 283–291.

15 C. De La Cruz, A. Molina, N. Patil, E. Ventosa, R. Marcilla and A. Mavrandonakis, *Sustain. Energy Fuels*, 2020, **4**, 5513–5521.

16 W. Lee, B. W. Kwon and Y. Kwon, *ACS Appl. Mater. Interfaces*, 2018, **10**, 36882–36891.

17 Q. Zhang, A. Khetan and S. Er, *Sci. Rep.*, 2020, **10**, 22149.

18 Q. Zhang, A. Khetan and S. Er, *Sci. Rep.*, 2021, **11**, 4089.

19 S. Er, C. Suh, M. P. Marshak and A. Aspuru-Guzik, *Chem. Sci.*, 2015, **6**, 885–893.

20 S. B. Kristensen, T. van Mourik, T. B. Pedersen, J. L. Sørensen and J. Muff, *Sci. Rep.*, 2020, **10**, 13571.

21 J. J. Irwin and B. K. Shoichet, *J. Chem. Inf. Model.*, 2005, **45**, 177–182.

22 Q. Zhang, A. Khetan, E. Sorkun, F. Niu, A. Loss, I. Pucher and S. Er, *Energy Storage Mater.*, 2022, **47**, 167–177.

23 A. Ghodbane, P. Bordat, N. Saffon, S. Blanc and S. Fery-Forgues, *Dye. Pigment.*, 2016, **125**, 282–291.

24 C. M. Fitchett, C. Richardson and P. J. Steel, *Org. Biomol. Chem.*, 2005, **3**, 498–502.

25 J. Hong, M. Lee, B. Lee, D. H. Seo, C. B. Park and K. Kang, *Nat. Commun.*, 2014, **5**, 5335.

26 C. Kaes, A. Katz and M. W. Hosseini, *Chem. Rev.*, 2000, **100**, 3553–3590.

27 M. Waki, Y. Maegawa, K. Hara, Y. Goto, S. Shirai, Y. Yamada, N. Mizoshita, T. Tani, W. J. Chun, S. Muratsugu, M. Tada, A. Fukuoka and S. Inagaki, *J. Am. Chem. Soc.*, 2014, **136**, 4003–4011.

28 X. Zhang and A. McNally, *ACS Catal.*, 2019, **9**, 4862–4866.

29 M. Sánchez-Castellanos, M. M. Flores-Leonar, Z. Mata-Pinzón, H. G. Laguna, K. M. Garciá-Ruiz, S. S. Rozenel, V. M. Ugalde-Saldívar, R. Moreno-Esparza, J. J. H. Pijpers and C. Amador-Bedolla, *Phys. Chem. Chem. Phys.*, 2019, **21**, 15823–15832.

30 Maestro, Schrödinger, LLC, New York, NY (2019).

31 K. Wedege, E. Dražević, D. Konya and A. Bentien, *Sci. Rep.*, 2016, **6**, 1–13.

32 J. D. Milshtein, L. Su, C. Liou, A. F. Badel and F. R. Brushett, *Electrochim. Acta*, 2015, **180**, 695–704.

33 A. D. Bochevarov, E. Harder, T. F. Hughes, J. R. Greenwood, D. A. Braden, D. M. Philipp, D. Rinaldo, M. D. Halls, J. Zhang and R. A. Friesner, *Int. J. Quantum Chem.*, 2013, **113**, 2110–2142.

34 M. G. Medvedev, I. S. Bushmarinov, J. Sun, J. P. Perdew and K. A. Lyssenko, *Science* , 2017, **355**, 49–52.

35 J. P. Perdew, K. Burke and M. Ernzerhof, *Phys. Rev. Lett.*, 1996, **78**, 3865–3868.

36 P. J. Hay and W. R. Wadt, *J. Chem. Phys.*, 1985, **82**, 299–310.

37 D. J. Tannor, B. Marten, R. Murphy, R. A. Friesner, D. Sitkoff, A. Nicholls, B. Honig, M. Ringnald and W. A. Goddard, *J. Am. Chem. Soc.*, 1994, **116**, 11875–11882.

38 R. E. Skyner, J. L. McDonagh, C. R. Groom, T. Van Mourik and J. B. O. Mitchell, *Phys. Chem. Chem. Phys.*, 2015, **17**, 6174–6191.

39 J. Koziol and D. E. Metzler, *Z. Naturforsch., B.*, 1972, **27**, 1027–1029.

40 T. Breton, D. Liaigre and E. M. Belgsir, *Electrochem. commun.*, 2005, **7**, 1445–1448.

41 M. Yan, Y. Kawamata and P. S. Baran, *Chem. Rev.*, 2017, **117**, 13230–13319.

42 E. Sorkun, Q. Zhang, A. Khetan, M. C. Sorkun and S. Er, https://doi.org/10.26434/chemrxiv.14398067.v1.[April 12, 2021]

43 W. Zhang, Y. Chen, T. R. Wu, X. Xia, J. Xu, Z. Chen, J. Cao and D. Y. Wu, *New J. Chem.*, 2022, **46**, 11662–11668.